Diffusion-Driven Pattern Formation in Ionic Chemical Solutions

Zsanett Viranyi, Ágota Tóth, and Dezső Horváth*

Department of Physical Chemistry, University of Szeged, P.O. Box 105, Szeged, H-6701, Hungary

(Received 6 August 2007; published 29 February 2008)

The driving force in diffusion-driven pattern formation is the difference in the diffusional flux of the key species, which in the case of ionic systems builds up a local electric field at the concentration gradients. The arising additional migrational flux not only decreases but also enhances the instability of the base state, depending on the charge distribution among the components. The opposite charges on the slower diffusing autocatalyst and its reacting counterpart favor pattern formation and shift the onset of instability to a smaller difference in the diffusion coefficients. The same charges, in addition to having the opposite effect, may even lead to the complete stabilization of planar reaction fronts unstable in the neutral system.

DOI: 10.1103/PhysRevLett.100.088301 PACS numbers: 82.40.Ck, 82.40.Qt, 82.45.Gj, 87.18.−h

Diffusion-driven instability represents one of the main driving forces in spatiotemporal pattern formation [1]. In a spatially distributed system of a chemical reaction, diffusion coupled with chemical kinetics may create concentration gradients by amplifying the ever-present microscopic perturbations [2–4]. The instability arises from the smaller diffusion rate of the species providing the positive feedback in the mechanism with respect to its counterpart. This long range inhibition (or short range activation) is responsible for the existence of a variety of spatiotemporal structures like Turing patterns [5,6], replicating spots [7,8], labyrinthine patterns [9,10], segmented waves [11], and cellular fronts [12–14].

The establishment of the necessary difference in diffusion coefficients is often the most difficult task in the experimental realization of spatial patterns. The common procedure involves the application of an immobile agent—generally embedded in a crosslinked polymer matrix—which reversibly binds the autocatalyst or activator in order to decrease the diffusive flux of the free species with respect to the other components [5,8,14–16].

In the majority of the experimental systems the key species are aqueous ions; therefore, a local electric field (Planck field) builds up as a result of the difference in diffusion coefficients [17,18]. The resultant diffusional potential leads to migrational fluxes that generally decrease the total flux of the species with a greater diffusion coefficient to maintain macroscopic charge balance [19]. The effective diffusion coefficient—applied generally for binary electrolytes—is, however, meaningless to systems where the composition varies in space.

In this work we are going to show that the local electric field arising in an ionic system yields migrational fluxes comparable to diffusional fluxes responsible for diffusion-driven pattern formation. The additional transport process will modify significantly both the onset and the extent of instability, which will be demonstrated in two of the spatiotemporal patterns mentioned above: Turing patterns, i.e., the stationary spatial structures in open systems, and cellular reaction fronts yielding transient patterns in closed systems. Although the effect of charged species on Turing instability has been addressed previously [20,21], it involved the assumption of constant transference numbers which is only applicable to spatially homogeneous systems and at the same time unappropriate for describing spatial patterns. In this study we have selected prototype models that possess the general features of the instability and for the first time we carry out rigorous stability analysis, which may generally be applied for other types of spatial pattern formation.

In a spatially distributed system of aqueous ions with a chemical reaction among them, the governing equations [17,19] are

$$\frac{\partial c_i}{\partial \tau} = \delta_i \nabla^2 c_i + z_i \delta_i \nabla(c_i \nabla \psi) + f_i(c_1, \ldots, c_n), \tag{1a}$$

$$0 = \sum_{i=1}^{n} [z_i \delta_i \nabla^2 c_i + z_i^2 \delta_i \nabla(c_i \nabla \psi)], \tag{1b}$$

where the dimensionless parameters and variables are defined as follows: the concentration of the species with charge z_i is scaled to an arbitrary reference value, $\delta_i = D_i/D$ represents the relative diffusivity with respect to a selected species (in the case of Turing instability it is the inhibitor, while for lateral instability it is the reactant), the dimensionless potential is given as $\psi = \Psi F/(RT)$, the time scale $\tau = t/t_s$, where t_s depends on the actual chemical model ($\boldsymbol{f}$) and the length scales $\xi = x/\sqrt{Dt_s}$, $\eta = y/\sqrt{Dt_s}$, defining ∇ as $(\partial/\partial\xi, \partial/\partial\eta)^T$. Equation (1b) represents the charge balance, since in aqueous solution electrostatic forces do not allow the macroscopic separation of charges under normal conditions.

In the case of Turing instability the homogeneous state under investigation is defined as the solution of $\boldsymbol{f}(\boldsymbol{c}) = 0$, yielding $\psi = 0$. For the linear stability analysis—in a one-dimensional system without loss of generality—we take the small spatial perturbation of this base state in the form of

$$c_i(\xi, \tau) = c_{i,0} + \sum_k c_{i,1,k} e^{\omega\tau + ik\xi}, \tag{2a}$$

$$\psi(\xi, \tau) = \sum_k \psi_{1,k} e^{\omega\tau + ik\xi}, \tag{2b}$$

 © 2008 The American Physical Society

where $c_{i,0}$ represents the homogeneous state. The first-order perturbation yields

$$\omega \begin{pmatrix} 1 & \dots & 0 & 0 \\ \dots & \dots & \dots & \dots \\ 0 & \dots & 1 & 0 \\ 0 & \dots & 0 & 0 \end{pmatrix} \begin{pmatrix} c_{1,1,k} \\ \dots \\ c_{n,1,k} \\ \psi_{1,k} \end{pmatrix} = \begin{pmatrix} -\delta_1 k^2 + J_{1,1} & \dots & J_{1,n} & -z_1 \delta_1 c_{1,0} k^2 \\ \dots & \dots & \dots & \dots \\ J_{n,1} & \dots & -\delta_n k^2 + J_{n,n} & -z_n \delta_n c_{n,0} k^2 \\ -z_1 \delta_1 k^2 & \dots & -z_n \delta_n k^2 & -\sum z_i^2 \delta_i c_{i,0} k^2 \end{pmatrix} \begin{pmatrix} c_{1,1,k} \\ \dots \\ c_{n,1,k} \\ \psi_{1,k} \end{pmatrix}, \quad (3)$$

written in matrix form, where $J_{i,j} = \partial f_i / \partial c_j$. This generalized eigenvalue problem can be solved to obtain the temporal eigenvalue ω as a function of the spatial wave number of the perturbation k and hence to construct the dispersion relation.

For this study the Schnakenberg model [22] is considered with various charges on the key species as listed in Table I. In this originally two-variable system, the two opposite cases are compared with the classic neutral model: in one the key components have the same charge, in the other they have opposite charge. In the modified schemes additional species (E, E_1, and E_2) are included to account for the charge balance as necessary but leaving the rate equations for X and Y unchanged. During the calculations, parameter values inside the region of Turing instability are selected, where the homogeneous steady state is stable to homogeneous perturbations. For Turing instability to occur, the autocatalyst X has to diffuse slower; therefore, $\delta_1 < 1$ is selected and the generalized eigenvalue problem in Eq. (3) is solved by the DGGEV routine provided in LAPACK in order to construct the dispersion curve. The original PDE's in Eq. (1) are also solved to calculate the concentration profiles and the potential field in a one spatial dimensional system with no-flux boundary conditions at the ends of an equally spaced grid of 1001 points with spacing $h = 0.01$. The integration of Eq. (1a) is carried out with the CVODE package [23], where ψ is obtained from Eq. (1b).

The dispersion curves show that charges on the intermediates mainly affects the temporal eigenvalue, while the wave number of the unstable modes varies insignificantly as shown in Fig. 1. Opposite charge on the key species increases ω and hence the region of unstable modes with respect to the neutral system. Same charge on X and Y, however, leads to stabilization; the critical ratio of diffusion coefficients—characterizing the onset of instability—therefore also depends on the distribution of charges on the species.

TABLE I. Investigated variations of the Schnakenberg model $r_1 = k_1$, $r_2 = k_2$, $r_3 = k_3 c_1^2 c_2$, $r_4 = k_4 c_1$, $(r_5 = k_5 c_3)$ with $k_1 = 0.001$, $k_2 = 0.01$, $k_3 = 2.57 \times 10^{-4}$, $k_4 (= k_5) = 1.4$.

Model 1	Model 2	Model 3
$A \to X$	$A \to X^+ (+E_2^-)$	$A \to X^- (+E^+)$
$B \to Y$	$B \to Y^- (+E_1^+)$	$B \to Y^- (+E^+)$
$2X + Y \to 3X$	$2X^+ + Y^- \to 3X^+ (+2E_2^-)$	$2X^- + Y^- \to 3X^-$
$X \to P$	$X^+ (+E_2^-) \to P_1$	$X^- (+E^+) \to P$
	$E_1^+ (+E_2^-) \to P_2$	

Although the homogeneous state is identical for all three models, the patterns that develop from spatial perturbations differ. Figure 2 demonstrates that opposite charges yield greater difference in the amplitude of the concentrations and leads to a negative phase shift in the local electric field strength with respect to the concentration distribution of the autocatalyst. On the other hand a positive phase shift occurs for identical charges on X and Y.

In case of lateral instability the base state is a planar reaction front propagating at a constant velocity u in the direction of the ξ-axis, i.e., the time-independent solution of

$$\frac{\partial c_i}{\partial \tau} = \delta_i \frac{\partial^2 c_i}{\partial \zeta^2} + u \frac{\partial c_i}{\partial \zeta} + z_i \delta_i \frac{\partial}{\partial \zeta} \left(c_i \frac{\partial \psi}{\partial \zeta} \right) + f_i(\boldsymbol{c}), \quad (4a)$$

$$0 = \sum_{i=1}^{n} \left(z_i \delta_i \frac{\partial^2 c_i}{\partial \zeta^2} + z_i^2 \delta_i \frac{\partial}{\partial \zeta} \left(c_i \frac{\partial \psi}{\partial \zeta} \right) \right), \quad (4b)$$

where the moving coordinate is defined as $\zeta = \xi - u\tau$. The boundary condition at $\zeta = +\infty$ corresponds to the reactant solution while at $\zeta = -\infty$ to the product of the reaction. The composition of the latter depends only on the stoichiometry of the reaction model as no external electric field is imposed. Both the concentration and the potential gradients vanish at $\zeta = \pm\infty$. For the linear stability analysis we apply a small spatial perturbation transverse to the direction of propagation, therefore the front position—the location of points with maximum rate of reaction—becomes $\zeta_p(\eta, \tau) = \sum_k \exp(\omega\tau + ik\eta)$, where for simplicity only the second spatial dimension is considered and k is the wave number associated with the perturbation.

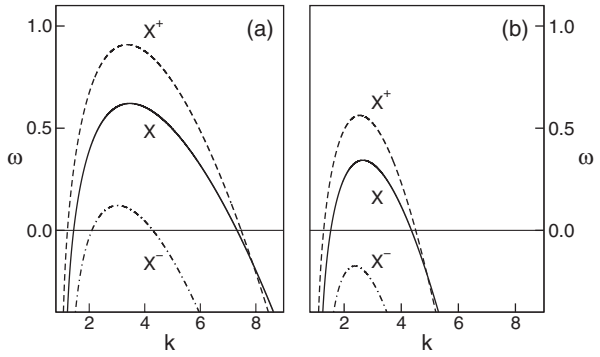

FIG. 1. Dispersion curves characterizing the stability of the homogeneous steady state for two selected sets of diffusion coefficients: (a) $\delta_1 = 0.02$ and (b) $\delta_1 = 0.05$. Solid lines represent the original (neutral) Schnakenberg model.

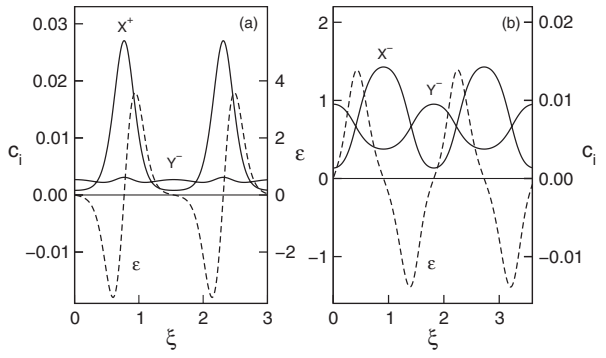

FIG. 2. Concentration profiles of the key species in the stationary Turing patterns for $\delta_1 = 0.01$ with (a) opposite and (b) identical charges. Also shown with dashed lines is the local electric field $\epsilon = -d\psi/d\xi$.

The concentration and the potential field may then be expressed as

$$c_i(\zeta, \eta, \tau) = c_{i,0}(\zeta) + \sum_k c_{i,1,k}(\zeta) e^{\omega\tau + ik\eta}, \tag{5a}$$

$$\psi(\zeta, \eta, \tau) = \psi_0(\zeta) + \sum_k \psi_{1,k}(\zeta) e^{\omega\tau + ik\eta}, \tag{5b}$$

where $c_{i,0}$ and $\psi_{i,0}$ represent the planar front, i.e., the time-independent solution of Eq. (4). The first-order terms decouple in Eq. (1) leading to

$$\begin{aligned}\omega c_{i,1,k} = {} & \delta_i c''_{i,1,k} + u c'_{i,1,k} + z_i \delta_i (c'_{i,0}\psi'_{1,k} + c'_{i,1,k}\psi'_0 \\ & + c_{i,1,k}\psi''_0 + c_{i,0}\psi''_{1,k} k^2 c_{i,0}\psi_{1,k}) \\ & - \delta_i k^2 c_{i,1,k} + g_{i,k},\end{aligned} \tag{6a}$$

$$\begin{aligned}0 = {} & \sum_{i=1}^{n} [z_i \delta_i (c''_{i,1,k} - k^2 c_{i,1,k}) \\ & + z_i^2 \delta_i (c'_{i,0}\psi'_{1,k} + c'_{i,1,k}\psi'_0 + c_{i,1,k}\psi''_0 + c_{i,0}\psi''_{1,k} \\ & - k^2 c_{i,0}\psi_{1,k})],\end{aligned} \tag{6b}$$

which is a generalized eigenvalue problem similar to Eq. (3), where $'$ denotes differentiation with respect to ζ and $g_{i,k} = \sum_{j=1} J_{i,j} c_{j,1,k}$.

In this work we consider cubic autocatalysis and compare the behavior of models with charged species with that of the neutral model [12,24]. We place the charge on the species so that the reactant and the autocatalyst have opposite or the same charge, where in the latter case we distinguish two possibilities: either the number of ions is unchanged in the course of the reaction or it increases (see Table II). There is a chemically inert counterion in models 2–4 (not shown in Table II) to account for the charge balance.

TABLE II. Investigated cubic models ($r = c_1 c_2^2$).

Model 1: $A \rightarrow B$	Model 2: $A^- \rightarrow B^+ + C^{2-}$
Model 3: $A^- \rightarrow B^- + C^+ + D^-$	Model 4: $A^- \rightarrow B^-$

The time-independent solution to Eq. (4) is obtained by a relaxation method on an equally spaced grid of 701 points with grid spacing $h = 0.1$. During the integration, the velocity of propagation u is adjusted according to $u = \int_{-\infty}^{+\infty} c_1 c_2^2 d\zeta$, i.e., the integral of Eq. (4a). The same discretization of Eq. (6) transforms the matrix operator into a regular banded matrix with a bandwidth of $2n + 1$.

For model 2 as the diffusion coefficient of the autocatalyst (δ_2) decreases, not only the region of unstable spatial modes increases as expected but also a positive local electric field builds up ahead of the reaction front. This local field leads to the enhanced flux of the reactant into the reaction zone further destabilizing the planar front similarly to migration-driven front instability [18], leading to greater δ_2 at the onset of instability. By comparing the dispersion curves to that of the neutral model (see Fig. 3), we can realize that opposite charges on the reactant and the autocatalyst increase the extent of instability by creating a positive local electric field ahead of the front, while identical charges on the key species have the opposite effect by building up a negative electric field. It is important to point out that complete stabilization occurs when no additional ions are produced in the course of the reaction (model 4) even with large difference in the diffusion coefficients, in which case the stabilizing migrational fluxes due to the stronger local field overwhelm the diffusional fluxes that would otherwise be responsible for the instability.

In this Letter we have shown that the local electric field arising due to the different diffusional rate of ions in a chemical reaction producing spatial patterns leads to the additional flux of the key species, that may both stabilize and further destabilize the base state, depending on the charge distribution among the components. As elucidated by considering two different instabilities, opposite charges on the autocatalyst and the reactive species result in an increase in the extent of instability originally present from differential diffusion, while identical charges lead to partial

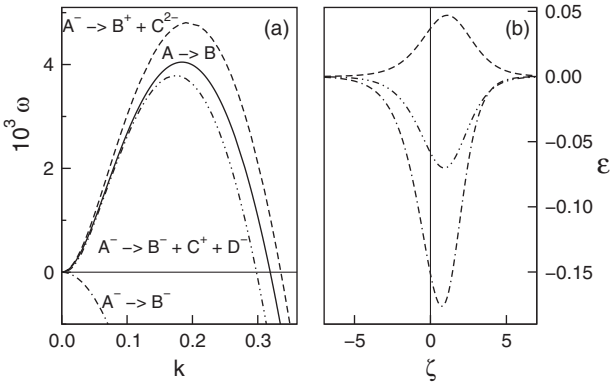

FIG. 3. Dispersion curves for each model at $\delta_2 = 0.2$ (a) with the corresponding local electric field at the reaction front (b).

stabilization. In the latter scenario complete stabilization of planar fronts may occur when no additional charged species are formed in the course of the reaction.

With respect to further reaction-diffusion systems, although the diffusion potential caused by the slower diffusion rate of the autocatalyst increases its apparent diffusion coefficient—which at first glance could only lead to partial or complete stabilization—, the local electric field also affects the flux of other species that may lead to smaller relative diffusion coefficients increasing the extent of diffusion-driven instability. Concerning the experimental systems, the presented results reveal that opposite charges in the key species are expected to facilitate diffusion-driven instability, while in reactions with the important components having the same charge a supporting electrolyte may be necessary to suppress the stabilizing effect that would otherwise arise due to the local field. In more complicated biological systems macromolecules and enzymes often appears as polyelectrolytes; therefore, migrational flux due to local electric field may especially be an important factor in spatiotemporal pattern formation.

This work is financially supported by the Hungarian Scientific Research Fund (OTKA, No. T46010).

*horvathd@chem.u-szeged.hu

[1] *Chemical Waves and Patterns*, edited by R. Kapral and K. Showalter (Kluwer, Dordrecht, 1995).
[2] A. M. Turing, Phil. Trans. R. Soc. B **237**, 37 (1952).
[3] Y. Kuramoto, in *Dynamics of Synergetic Systems. Proceedings of the International Symposium on Synergetics*, edited by H. Haken (Springer, Berlin, 1980), p. 134.
[4] W. van Saarloos, Phys. Rep. **386**, 29 (2003).
[5] V. Castets, E. Dulos, J. Boissonade, and P. De Kepper, Phys. Rev. Lett. **64**, 2953 (1990).
[6] I. Lengyel and I. R. Epstein, Science **251**, 650 (1991).
[7] J. E. Pearson, Science **261**, 189 (1993).
[8] K. J. Lee, W. D. McCormick, J. E. Pearson, and H. L. Swinney, Nature (London) **369**, 215 (1994).
[9] K. J. Lee, W. D. McCormick, Q. Ouyang, and H. L. Swinney, Science **261**, 192 (1993).
[10] A. Kaminaga, V. K. Vanag, and I. R. Epstein, J. Chem. Phys. **122**, 174706 (2005).
[11] V. K. Vanag and I. R. Epstein, Proc. Natl. Acad. Sci. U.S.A. **100**, 14 635 (2003).
[12] D. Horváth, V. Petrov, S. K. Scott, and K. Showalter, J. Chem. Phys. **98**, 6332 (1993).
[13] D. Horváth and Á. Tóth, J. Chem. Phys. **108**, 1447 (1998).
[14] P. W. Davies, P. Blanchedeau, E. Dulos, and P. De Kepper, J. Phys. Chem. A **102**, 8236 (1998).
[15] D. Horváth and K. Showalter, J. Chem. Phys. **102**, 2471 (1995).
[16] Á. Tóth, B. Veisz, and D. Horváth, J. Phys. Chem. A **102**, 5157 (1998).
[17] S. Schmidt and P. Ortoleva, J. Chem. Phys. **67**, 3771 (1977).
[18] Z. Virányi, Á. Tóth, and D. Horváth, J. Eng. Math. **59**, 229 (2007).
[19] J. Newman and K. E. Thomas-Alyea, *Electrochemical Systems* (Wiley, Hoboken, 2004), 3rd ed.
[20] J. Jorné, J. Theor. Biol. **55**, 529 (1975).
[21] H. Malchow, Physica (Amsterdam) **213A**, 159 (1995).
[22] J. Schnakenberg, J. Theor. Biol. **81**, 389 (1979).
[23] S. D. Cohen and A. C. Hindmarsh, Comput. Phys. **10**, 138 (1996).
[24] A. Malevanets, A. Careta, and R. Kapral, Phys. Rev. E **52**, 4724 (1995).